PLEASE CITE THIS ARTICLE AS DOI: 10.1122/8.0000085

Flow driven transitions of polyelectrolytes

Sunil P. Singh^{1, a)} and Roland G. Winkler²

Indian Institute Of Science Education and Research, Bhopal 462 066, Madhya Pradesh, India

²⁾Theoretical Physics of Living Matter, Institute for Advanced Simulation, Forschungszentrum Jülich, 52425 Jülich, Germany^{b)}

The nonequilibrium properties of uniformly charged linear polymers in the presence of explicit counterions under shear flow are studied by coarse-grained mesoscale hydrodynamics simulations. The conformational properties of the polyelectrolyte (PE) are quantified by the gyration tensor, the distribution of the end-to-end distance, and alignment with the flow, which display rather universal behavior for small and moderate electrostatic interaction strengths in regime of condensed counterions. In the limit of strong counterion condensation, shear flow leads to a globule-coil transition and polymer stretching, associated with an increase of the effective PE charge. The polyelectrolytes exhibit a pronounced tumbling motion with cyclic stretched and collapsed conformations. The average tumbling-time period decreases with increasing shear rate by a power-law with the exponent -2/3 for PEs in the coiled state. The tumbling time exhibits a plateau-like regime over nearly a decade of shear rates for PEs in the globular state. In addition, we identify various characteristic PE structures under flow in the globule and coil limits determined by the condensed counterions.

I. INTRODUCTION

Soft polymeric macromolecules respond to external perturbations in an intriguing way, and exhibit numerous features which are non-intuitive and distinct from those at equilibrium.^{1–4} In particular, a non-monotonic structural response of polymers and ultra-soft colloids under sedimentation has been observed^{5–9}, molecular mass independent mobilities of charged polymers^{4,10–14}, aperiodic tumbling dynamics under linear flow^{1,2,15–20}, globule-to-coil transitions or vice-versa^{21–23}, migration of polymers toward a wall in parabolic flow^{24,25}, and many more effects. The understanding of the various non-equilibrium characteristics of flexible macromolecules under flow is vital for numerous reasons, *viz.* rheological properties of polymer solutions^{26,27}, transport through nanopores^{4,28}, oil recovery²⁹, biomedical applications^{21,22,30–33}, etc.

There is a large amount of literature on the flow behavior of neutral dilute and semidilute polymer suspensions $^{1,2,15-18,34-37},$ which unveils their nonequilibrium structural and dynamical properties. A particular example is the shear driven globule-to-coil transition of the von Willebrand factor, which plays a crucial role in the blood clotting in narrow arteries at relatively high shearrates $(\dot{\gamma}=10^4s^{-1}),^{21,22,33}$ where the von Willebrand factor fibers suddenly open up in the stretched form and undergo large-scale conformational changes. The open-state mediates adhesion and aggregation via cross-linking of platelets on the surface of arteries 21,33 .

Various approaches have been applied to shed light onto the equilibrium and nonequilibrium physical aspects of polyelectrolytes (PE). In a simplified description, electrostatic interactions are accounted for by the Debye-Hückel potential taking counterions into account implicitly only^{4,38–42}.

Moreover, more detailed bead-spring polyelectrolyte models are employed, which take counterions and long-range Coulomb interactions explicitly into account^{4,11–14,23,28,42–47}. Specifically, the dependence of the nonmonotonic equilibrium structural properties on the solvent quality^{28,43-46}, the bulk electrophoretic response with molecular-mass independent mobility^{4,11-14}, as well as confinement effects on the structure and relaxation behavior of polyelectrolytes have been addressed^{47–50}. Polyelectrolytes confined in a channel and exposed to pressure-driven flow reveal transverse migration^{38,51–53}. In addition, the conformational properties of polyelectrolyte chains adsorbed on surfaces has been studied 39-41,54,55, and tank-treading and tumbling dynamics of circular polyelectrolyte in extensional and linear flow has been observed^{56,57}. However, studies on the behavior of bulk polyelectrolytes under shear flow are rare^{57,58}, in particular, the influence of explicit counterions and the coupling of longrange electrostatic and hydrodynamic interactions are unresolved. The present study sheds light onto the coupling of polyelectrolyte conformations, its nonequilibrium dynamics, and charge effects in linear shear flow, aspects relevant for a wide class of biopolymers⁵⁸ and synthetic polymers.

In this article, we present a detailed study of the structural and dynamical properties of polyelectrolytes in presence of counterions under shear flow. We apply a hybrid coarse-grained simulation approach, combining molecular dynamics simulations of the PE and its counterions with the multiparticle collision dynamics method for the explicit fluid^{59,60}. In particular, this approach captures the fluid-mediated interactions between a PE and its counterions. Moreover, long-range electrostatic interactions are taken into account, which tightly couple the PE and counterion structure and dynamics^{14,28,43,44}. The long-range nature of electrostatic and fluid-mediated interactions, on the one hand, renders a detailed understanding of the multicomponent system rather intricate, but, on the other hand, yields features, which are absent in a comparable uncharged system.

Polyelectrolytes show large-scale conformational changes under shear-flow. Yet, we find that structural and dynami-

¹⁾ Department of Physics,

a) Electronic mail: spsingh@iiserb.ac.in

b) Electronic mail: r.winkler@fz-juelich.de

PLEASE CITE THIS ARTICLE AS DOI: 10.1122/8.0000085

cal properties exhibit universal behavior with respect to the shear rate, when represented as function of the Weissenberg number $Wi = \dot{\gamma}\tau$, where $\dot{\gamma}$ is the shear rate and τ a PE characteristic relaxation time, despite very different physical conditions. In particular, this applies to the shear-induced alignment, asphericity, and the tumbling dynamics. The counterions play an important role, especially for strong Coulomb interactions, when counterion condensation leads to compact globular structures. 43,45,46 Here, shear flow implies a globule-to-coil transition and even highly stretched conformations at large Weissenberg numbers. The observed transition is associated to hydrodynamic-drag and is reminiscent to globule-to-coil transitions of neutral polymers under badsolvent conditions.⁶¹ This globule-to-coil transition strongly affects the tumbling dynamics, which we characterize by the tumbling time determined from the time, which is required to flip the end-to-end vector by 2π . For low Coulomb interaction strengths, we obtain a universal Weissenberg-number dependence with the power-law relation $Wi^{-2/3}$, consistent with results for uncharged linear^{2,16,18,62,63} and star polymers.^{19,20} However, in the globule-to-coil transition regime, we find a plateau, where the tumbling time is essentially independent of the shear rate, before it drops as for lower Weissenberg numbers. This reflects a tight link between the polymer-counterion-aggregate conformations and its internal and global dynamics.

The article is organized as follows. In Sec. II the model of the polymer, the simulation approach for the fluid, and the implementation of long-range interaction (Lees-Edwards boundary conditions) are presented. In Sec. III and IV, the structural properties the PEs at equilibrium and under flow are discussed. Their dynamical aspects are presented in Sec. V. Finally, Sec. VI summaries our findings.

MODEL AND SIMULATION METHOD

Polymer and Counterions

We consider a coarse-grained representation of a uniformly, negatively charged, linear polymer chain with its monovalent counterions embedded in an electrically neutral fluid under shear flow (cf. Fig. 1). The chain consists N_m identical repeating units—denote as monomers—linked by the harmonic bond potential

$$U_b = \frac{k_s}{2} \sum_{i=1}^{N_m - 1} (|\mathbf{R}_i - \mathbf{R}_{i+1}| - l_0)^2,$$
 (1)

where R_i denotes the position of monomer $i, i = 1, ..., N_m, l_0$ the equilibrium bond length, and k_s the strength of the potential. The counterions are identical to the PE monomers except for their opposite charge with respect to the PE monomers. The number of counterions is equal to the number of monomers, $N_c = N_m$, i.e. the total system is neutral. To account for volume exclusion and to prevent bond crossing, all monomers and counterions interact via the repulsive and

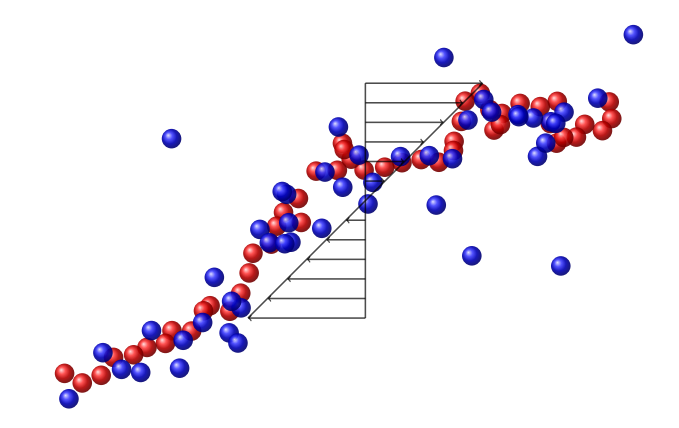


FIG. 1. Snapshot of a polyelectrolyte (red) with its counterions (blue). Arrows indicate the flow in the shear-gradient plane, with flow in the x- and the gradient in the y-direction of the Cartesian reference system.

truncated Lennard-Jones (LJ) potential

$$U_{LJ} = 4\varepsilon_{LJ} \sum_{i=1}^{N} \sum_{j \neq i=1}^{N} \left\{ \left(\frac{\sigma}{R_{ij}} \right)^{12} - \left(\frac{\sigma}{R_{ij}} \right)^{6} + \frac{1}{4} \right\}$$
 (2)

for $R_{ij} < \sqrt[6]{2}\sigma$ and zero otherwise, with $N = 2N_m$ the total number of solute particles, ε_{LJ} the strength of the potential, σ the particle diameter, and $R_{ij} = |\mathbf{R}_i - \mathbf{R}_i|$ the distance between a pair of particles. Alternative ways to account for polymer non-crossability have been suggested⁶⁴.

The Coulomb potential of the charged particles in presence of periodic boundary conditions is

$$U_c = \sum_{i,j=1}^{N} \sum_{n} \frac{1}{4\pi\varepsilon} \frac{q_i q_j}{R'_{ij}}$$
 (3)

where q_i is the charge of the *i*th particle, for a monomer $q_i = -e$, while for counterion $q_i = e$, e is the elementary charge, and ε is the permittivity. The summation over naccounts for all the periodic images of the primary box, 65 where the prime in the summation indicates omission of the i=j term for n=0, and $R'_{ij}=|R_j-R_i-L_n|$. Here, $L_{n\beta}=L_{\beta}n_{\beta}$, with L_{β} the extension of the cuboidal simulation box in the Cartesian direction β , and $n = (n_x, n_y, n_z)^T$ is an integer triplet. The detailed description of force calculation from electrostatic interactions using generalized Ewald summation is presented in Ref. 66. For the simplicity, the permittivity is assumed to be constant throughout the medium. The particles' dynamics is described by Newtons equations of motion, which are solved by the velocity-Verlet algorithm.⁶⁵

B. Fluid: Multiparticle Collision Dynamics (MPC)

A PE and its counterions are embedded in a coarse-grained fluid to account for possible fluid-mediated interactions and to impose the shear flow. As simulations have shown¹⁴, even in electrophoresis hydrodynamic interactions affect the dynamical properties of a PE.

PLEASE CITE THIS ARTICLE AS DOI: 10.1122/8.0000085

The dynamics of the N_f point-particles of the MPC fluid proceeds in two steps, streaming and collision^{59,60,67}. In the streaming step, the MPC particles move ballistically over a time interval h and their positions, r_k , are update as $r_k(t+h) = r_k(t) + hv_k(t)$, with t the time and v_k the velocity of particle k ($k = 1, \ldots, N_f$). In the collision step, MPC particles interact with each other as well as with monomers and counterions. For this purpose, all particles—MPC particles, monomers, and counterions—are sorted into cubic cells of side length a of a collision lattice. Their relative velocities with respect to the center-of-mass velocity of the cell are rotated by an angle α around a randomly oriented axis independently for every cell, i.e.,

$$\mathbf{v}_k(t+h) = \mathbf{v}_k(t) + (\mathcal{A}(\alpha) - \mathcal{I})(\mathbf{v}_k(t) - \mathbf{v}_{cm}(t)), \quad (4)$$

where \mathscr{A} is the rotation and \mathscr{I} is the unit matrix.^{67,68} The center-of-mass velocity of the MPC cell of particle k is

$$v_{cm}(t) = \frac{\sum_{i=1}^{N_c} m v_i(t) + \sum_{j=1}^{N_c^m} M V_j(t)}{m N_c + M N_c^m}$$
 (5)

for the N_c solvent particles (MPC solvent) and the N_c^m solute particles (monomers and/or counterions) of mass m and M, respectively. Rotation of the solute particle velocities according to Eq. (5) yields momentum exchange between the MPC fluid, the embedded PE and counterions, and *vice versa*, ^{59,60,67} providing the correct polymer dynamics ^{13,60}. The discretization of space in collision cells implies violation if Galilean invariance, which is reestablished by performing a random shift of the collision lattice ⁶⁹.

The linear shear flow of the form $v_x = \dot{\gamma} y$ is imposed by Lees-Edwards boundary conditions. 34,65,70 Here, images of the primary simulation box along the gradient direction move with constant relative velocity $v_x = n_y \dot{\gamma} L_y$ along the flow direction, where L_y is the box length in the gradient direction. When a particle (MPC solvent, monomer, counterion) leaves the primary box along the gradient direction, it is reinserted at the opposite side with a shifted position and the shifted velocity $\pm \dot{\gamma} L_y$. 65,67,70 . In the other spatial directions, boundary conditions are identical to the no-flow case. An external force imposing flow results in an increase of the temperature in the system. To maintain a desired temperature, a local thermostat is employed, which takes out the excess energy locally and ensures a Maxwellian velocity distribution 67 .

C. Simulation Parameters

Dimensionless quantities are introduced by scaling length by the bond length l_0 , energy by k_BT , and time by $\tau = \sqrt{ml_0^2/k_BT}$, where k_B is the Boltzmann factor and T the temperature. We choose the collision time $h=0.1\tau$, the rotation angel $\alpha=130^\circ$, and the mean number of MPC particles per collision cell $\langle N_c \rangle = 10$, which corresponds to the solvent viscosity $\eta=8.7\sqrt{mk_BT/l^{460,71,72}}$. Moreover, we set m=1, M=10m, $a=l_0$, $\sigma/l_0=0.8$, $\varepsilon_{LJ}/k_BT=1$, $k_s/(k_BT/l_0^2)=10^3$, and the time step for the integration of

Newtons equations of motion to $5 \times 10^{-3} \tau$. The choice of solute mass M and collision time h ensures a suitable hydrodynamic coupling between the solute and MPC fluid particles⁶⁰. The strength of the Coulomb interaction is measured by the Bjerrum length l_B , which is in units of l_0 , $l_B = e^2/(\varepsilon k_B T l_0)$. We consider the range of Bjerrum lengths $1 \le l_B \le 20$, where the variation of l_B is due to variations in the dielectric constant of the medium. All the simulations are performed for at least $1.25 \times 10^5 \tau$ time units after equilibration of the structure. A cubic simulation box of length L is used, where $L/l_0 = 50$ for $N_m = 50$ and $L/l_0 = 64$ for $N_m = 100$. Each simulation data point is averaged over at least 30 independent runs. If not indicated otherwise, the results are for the polymer length $N_m = 50$.

III. EQUILIBRIUM PROPERTIES

The equilibrium properties of a PE depend, in particular, on the Bjerrum length. As a reference for the characterization of nonequilibrium features of PEs, Fig. 2 displays the mean square end-to-end distance $\langle R_e^2 \rangle$, the radius of gyration $\langle R_g^2 \rangle$, as well as the relaxation times τ_r and τ_{rg} of these quantities, where $R_e = R_N(t) - R_1(t)$ and

$$\langle R_g^2 \rangle = \frac{1}{N_m} \sum_{i=1}^{N_m} \langle (\mathbf{R}_i - \mathbf{R}_{cm})^2 \rangle, \tag{6}$$

with the polymer center of mass R_{cm} . As is well know, in dilute solution $\langle R_e^2 \rangle$ and $\langle R_g^2 \rangle$ increase with increasing l_B until counterion condensation sets in at $l_B \approx 1$; a further increase, $l_B > 1$, leads to shrinkage of the PE. ^{43,45,46} In the limit of strong electrostatic interactions, $l_B > 10$, the PE attains a globular structure, which exhibits the weak dependence $R_g \sim l_B^{-1/5}$ on the Bjerrum length. ⁴⁵

The longest PE relaxation time follows from the end-to-end vector correlation function $C_e(t) = \langle \hat{R}_e(t) \cdot \hat{R}_e(0) \rangle$ (here $\hat{R}_e = R_e/|R_e|$), which decays exponentially with the characteristic time τ_r . Figure 2 displays relaxation times as function of Bjerrum length. The relaxation time rapidly decreases with increasing l_B as the globular state is approached. Apparently, in the globular regime, τ_r nearly saturates, as a consequence of small variations of end-to-end distance in the compact and dense state.

Alternatively, a relaxation time can be determined from the fluctuations of the radius of gyration via the correlation function

$$C_g(t) = \frac{\langle \delta R_g^2(t) \delta R_g^2(0) \rangle}{\langle \delta R_g^2(t) \rangle \langle \delta R_g^2(0) \rangle} = \exp(-t/\tau_{rg}), \tag{7}$$

where $\delta R_g^2(t) = R_g^2(t) - \langle R_g^2 \rangle$. Interestingly, the relaxation time τ_{rg} exhibits a non-monotonic dependence on l_B (cf. Fig. 2). In the limit of small l_B , τ_{rg} grows and after reaching a maximum at $l_B \approx 5$, it declines while the PE assumes the globular state. Naturally, τ_r is always larger, because it characterizes relaxation on larger scales. The initial growth of τ_{rg} reflects the small structural fluctuations in

PLEASE CITE THIS ARTICLE AS DOI: 10.1122/8.0000085

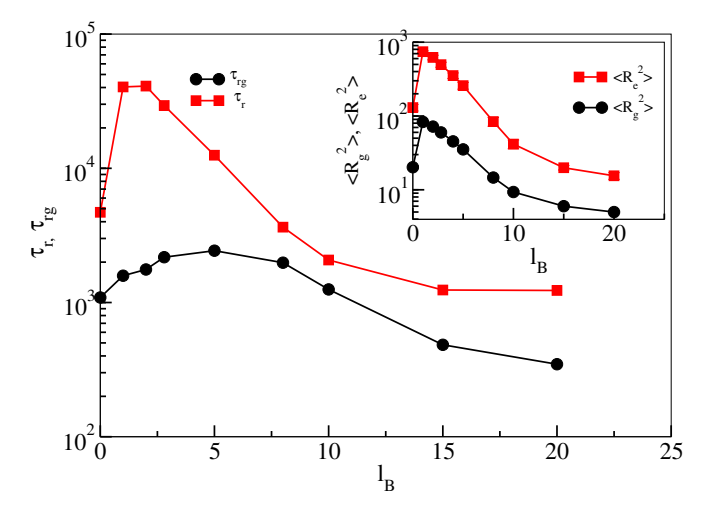


FIG. 2. Relaxation times τ_r and τ_{rg} of the radius-of gyration $\langle R_g^2 \rangle$ and the end-to-distance $\langle R_e^2 \rangle$, respectively, of PEs as a function of Bjerrum length l_B . The inset shows the mean square radius-of-gyration (\bullet) and the mean square end-to-end distance (\blacksquare) of the PE as a function of l_B .

the extended state. The fluctuations increase with increase of l_B , since counterion-mediated monomer-monomer attraction leads to more compact conformations. However, the fluctuations of the charge distribution implies considerable variation in the repulsive monomer-monomer Coulomb interaction with correspondingly enhanced conformational fluctuations. The counterion fluctuations decrease with increasing l_B , which implies a reduction of τ_{rg} in the globule limit, and also a slower drop of R_g .

IV. FLOW-INDUCED STRUCTURAL PROPERTIES

Polyelectrolytes show substantial conformational changes in response to the shear flow, along with a strong flow alignment. In particular, the PE conformations at large l_B are determined by its intimate coupling with condensed counterions.

A. Gyration Tensor

The shear-induced shape of the PEs is characterized by the average radius of gyration tensor

$$G_{\alpha\beta} = \frac{1}{N_m} \sum_{i=1}^{N_m} \langle \delta R_{i\alpha} \delta R_{i\beta} \rangle,$$
 (8)

where $\delta R_{i\alpha} = R_{i\alpha} - R_{cm\alpha}$ is the position of the *i*th monomer w.r.t. to center of mass of a PE.

Figure 3 displays the radius-of-gyration-tensor components along the flow and vorticity direction as a function of the Weissenberg number Wi. We use the Weissenberg number $Wi = \dot{\gamma}\tau_r$ to characterize the PE properties for $l_B < 5$ and $Wi = \dot{\gamma}\tau_{rg}$ for $l_B > 5$. With increasing Wi, G_{xx} swells monotonically as displayed in Fig. 3(a) for $\Delta G_{xx} = G_{xx} - G_{xx}^0$, with G_{xx}^0

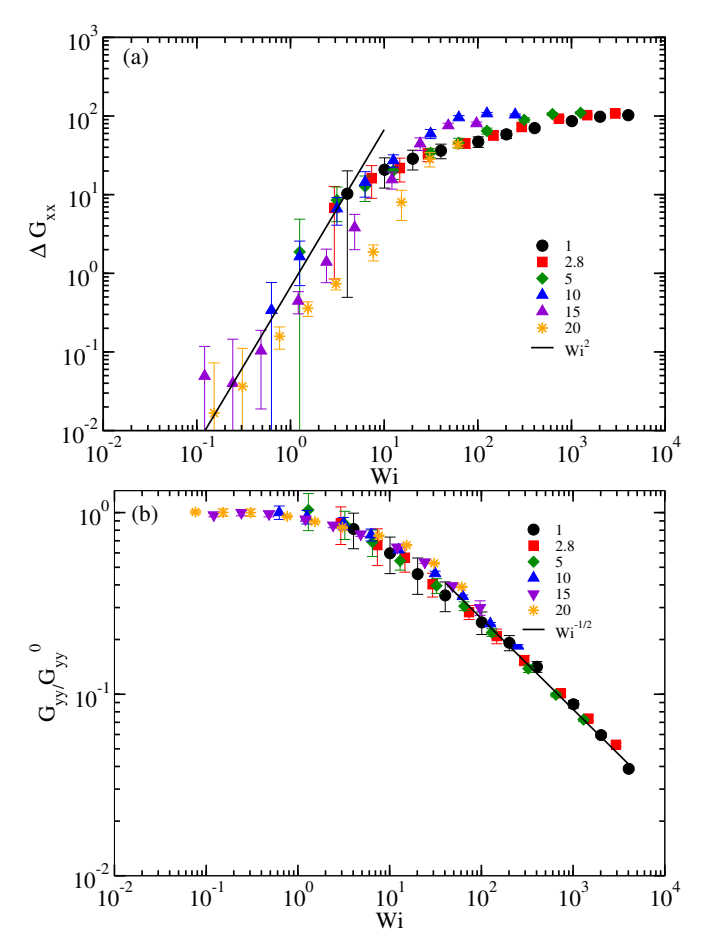


FIG. 3. Radius-of-gyration-tensor components (a) along the flow direction and (b) along the gradient direction as a function of the Weissenberg number, where the Weissenberg number is defined as $Wi = \dot{\gamma}\tau_r$ for $l_B \lesssim 5$ and $Wi = \dot{\gamma}\tau_{rg}$ for $l_B > 5$, respectively. The solid line in (a) shows a quadratic increase and that in (b) the decrease $Wi^{-1/2}$ with increasing Bjerrum length. The symbols corresponds to $l_B = 1$ (\bullet), $2.8(\blacksquare)$, $5(\spadesuit)$, $10\spadesuit$), $15(\blacktriangledown)$, and 20 (*).

the radius-of-gyration-tensor component at zero shear rate. The initial slope, $\Delta G_{xx} \sim Wi^2$, agrees with that of neutral polymers. 18,34,73–75 At high shear rates, ΔG_{xx} approaches a plateau. Evidently, the curves for $l_B < 5$ exhibit universal behavior over the full Wi range. No scaling is obtained for $l_B > 5$, especially for $l_B = 20$ and $Wi \lesssim 10$. For $l_B > 10$, the increase in ΔG_{xx} is weaker over the range $1 \lesssim Wi \lesssim 10$ as a consequence of strong PE-counterion interactions and the globular PE conformation. In general, the globule is nonspherical and shear leads to its alignment. Only above a certain, Bjerrum-length-dependent Weissenberg number, the globule is extended, and for sufficiently strong flow rates the asymptotic plateau values of the weaker l_B is reached. This transition is similar to the globule-coil transition of polymers in a bad solvent. Note that ΔG_{xx} for $l_B = 10$ and 15 reach the asymptotic plateau at lower $Wi=\dot{\gamma} au_{rg}$ than those for $l_B<5$ because of the different Weissenberg-number definitions.

The normalized gyration-tensor component in the shear gradient direction, G_{yy}/G_{yy}^0 , decreases with increasing Weis-

PLEASE CITE THIS ARTICLE AS DOI: 10.1122/8.0000085

senberg number (cf. Fig. 3(b)), in a nearly universal manner for the various l_B , despite the different definitions of Wi for $l_B \leq 5$, respectively. The decline of G_{yy} obeys the power-law $G_{yy} \approx Wi^{-1/2}$, comparable to that of neutral polymers.³⁴

B. Distribution of the Polymer End-to-End Distance

The flow-induced changes of the distribution function of the polymer end-to-end distance are illustrated in Fig. 4 and 5. As shown in Fig. 4(a), the distribution function for $l_B=2.8$ is close to a Gaussian at low flow strengths with a peak at $R_e\approx 24$. With increasing Wi, the peak shifts to larger R_e values, with the peak localized nearly at the maximum extension of the polymer in the limit $Wi\gg 1$. For $l_B=10$, the narrow peak at $R_e\approx 5$ reflects the globular structure of the polymer by its condensed ions. An increasing shear causes a gradual reduction of the peak height and the formation of a tail at larger R_e , however, no peak at large R_e emerges, but the distribution is rather flat with equal probability for nearly all end-to-end distances. The latter suggests strong fluctuations of the end-to-end distance.

Figure 5 displays two-dimensional probability distribution functions in the shear-gradient plane. For $l_B=1$, maxima of the end-to-end distance are clearly visible, whereas for $l_B=10$ and 20 the PEs are in a more globular state. The qualitative difference between the shear-rate response at small and large Bjerrum lengths reflects the presence of distinctly different PE confirmations, which are governed by the condensed counterions.

C. Effective Charge

Shear affects the amount of counterions in the vicinity of the PEs and, thus, their effective charge. We define the effective charge α via the number of counterions, N_a , within the cut-off distance $R_c = 2$ around the various monomers, hence $\alpha = 1 - N_a/N_m$. The inset of Fig. 6 displays the effective charge of equilibrium PEs as function of l_B . At smaller l_B , α is close to unity. However, in the limit $l_B \gg 1$, all counterions are adsorbed onto the polymer and $\alpha \approx 0.43$ Shear flow affects the effective charge for large $l_B > 10$ only weakly (cf. Fig. 6). Specifically, for $l_B = 20$, α is nearly constant and it is akin to the equilibrium number, i.e., all counterions are condensed. An increasing shear rate reduces the amount of condensed counterions for moderate Bjerrum lengths. Interestingly, the change of the effective charge, $\Delta \alpha = \alpha - \alpha_0$, is a non-monotonic function of the Bjerrum length, with a maximum in the vicinity of $l_B = 10$.

Figure 7 depicts the counterion distribution in the shear-gradient plane, which is reminiscent to the monomer distribution of neutral polymers. As expected, the distribution of ions weakly aligns with the flow for small Wi = 0.3, breaking the spherical symmetric of the system, but becomes strongly stretched in the large-shear limit Wi > 3000, e.g., for $l_B = 2.8$. Overall, the counterion distribution indicates a similar behavior as the monomers.

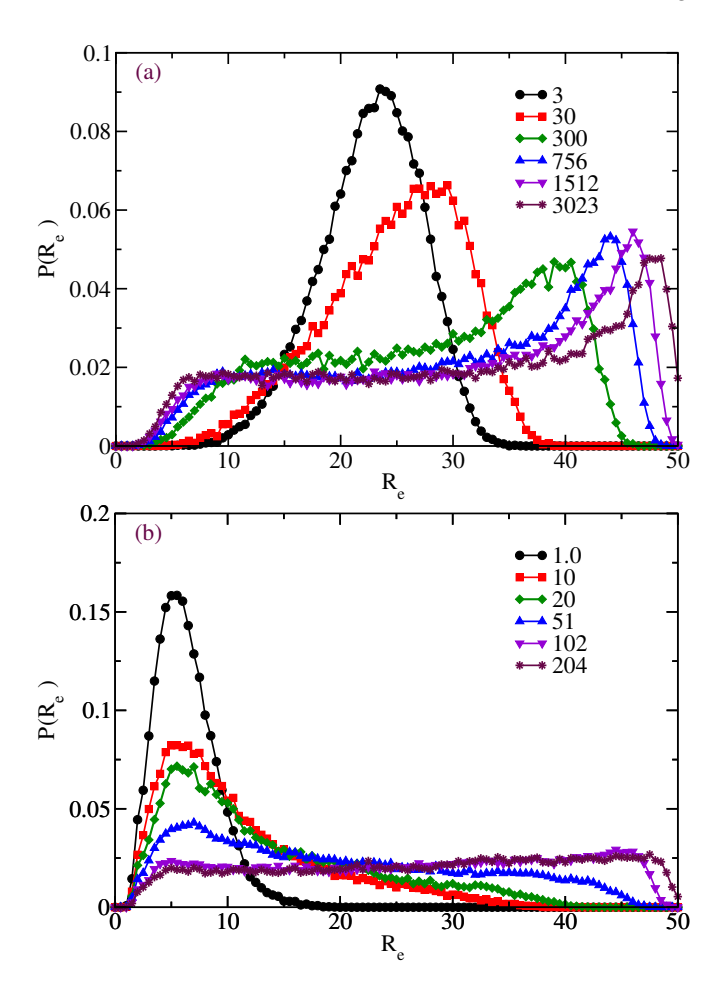


FIG. 4. Distribution function $P(R_e)$ of the polymer end-to-end distance R_e for the Weissenberg numbers indicated in the legends and the Bjerrum lengths (a) $l_B = 2.8$ and (b) $l_B = 10$.

D. Flow Induced Alignment

Flow leads to a preferred alignment of the polyelectrolyte, as displayed in Fig. 5, which is quantified by the angle ϕ between the eigenvector of the gyration tensor with the largest eigenvalue and the flow direction and can be expressed by the radius-of-gyration tensor components as 15,34

$$\tan \phi = \frac{2G_{xy}}{G_{xx} - G_{yy}}. (9)$$

In case of a PE, the shear-induced alignment is not only governed by Wi, but also electrostatic interactions play a significant role. This is reflected in Fig. 8, with the two groups of similarly behaving PEs, namely for $l_B \lesssim 5$ and for $l_B > 5$. We like to emphasize that scaling for coiled and globular PEs, respectively, is only obtained for the definition of the Weissenberg number in terms of the relaxation times τ_r and τ_{rg} , respectively—no scaling is obtained for $l_B > 5$ in case of $Wi = \dot{\gamma}\tau_r$. Evidently, the globular and coiled PEs exhibit a similar dependence on the Weissenberg number. In the limit of vanishing shear, ϕ is close to the equilibrium value $\pi/4$. Two power-law regimes can be identified for larger Wi,

PLEASE CITE THIS ARTICLE AS DOI: 10.1122/8.0000085

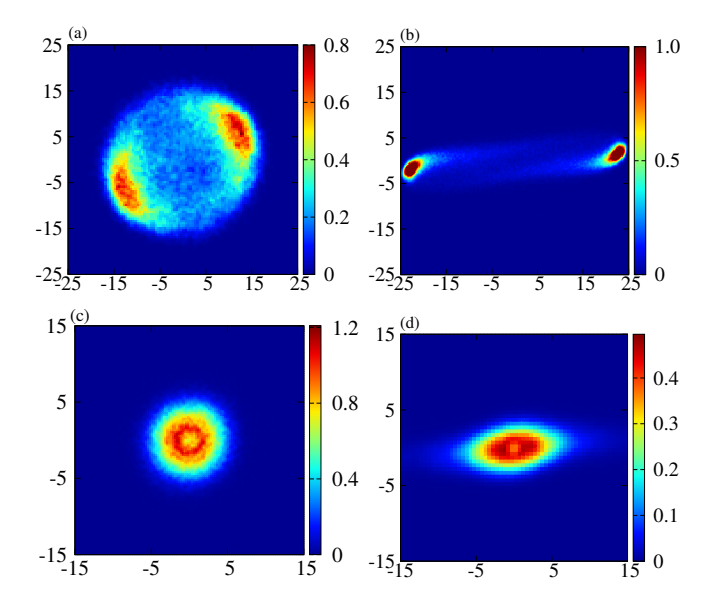


FIG. 5. Polyelectrolyte end-to-end vector distribution function (polymer center-of-mass reference frame) in the shear-gradient plane for (a) $l_B = 1$, Wi = 39.5, (b) $l_b = 1$, Wi = 1975, (c) $l_B = 20$, Wi = 1.24, and (d) $l_B = 20$, Wi = 62.

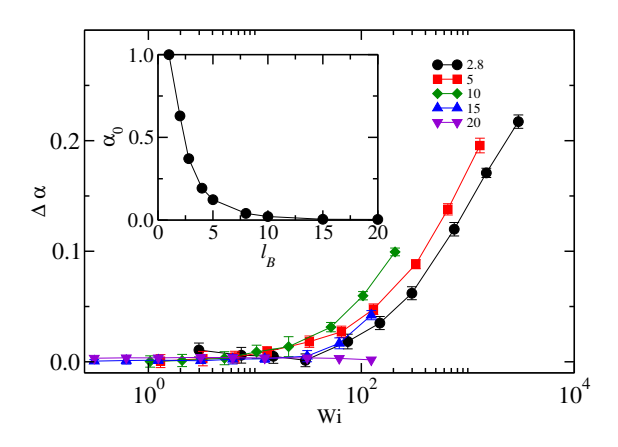


FIG. 6. Dependence of effective charge $\Delta \alpha = \alpha - \alpha_0$, $\alpha = 1 - N_a/N_m$, of PEs on the Weissenberg number Wi for $l_B = 2.8$, 5, 10, 15, and 20 (see legend). The cut-off distance between a polymer monomer and a condensed counterion is $R_c = 2$. The inset displays the effective charge α_0 of PEs at equilibrium as function of the Bjerrum length. Note that for all Bjerrum lengths the Weissenberg number is defined as $Wi = \dot{\gamma}\tau_r$.

namely $\tan \phi \sim W i^{-2/3}$ for $W i \lesssim 10$ and $\tan \phi \sim W i^{-1/3}$ for W i > 50.

E. Polyelectrolyte Conformations

In order to achieve a molecular understanding of the PE properties under flow, we classify the PE conformations in the following groups: stretched or extended state, a partially folded state, a U-shaped or folded state from both sides, which can be an open U or a collapsed form, a hair-pin or S-shape, which again can be of open or collapsed form, and globule and

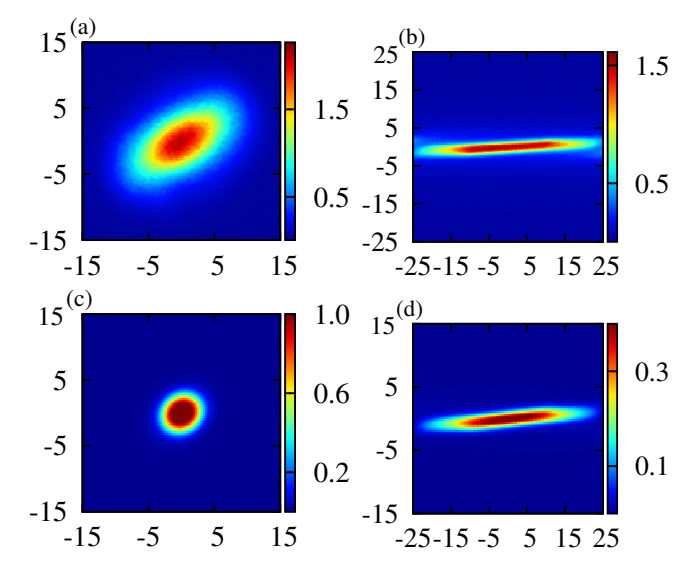


FIG. 7. Distribution of counterions w.r.t. the polymer center-of-mass in the shear-gradient plane. (a) $l_B=2.8$ and Wi=0.3, (b) $l_B=2.8$ and Wi=3023, (c) $l_B=10$ and Wi=1.05, (d) $l_B=10$ and Wi=209. Note that for all Bjerrum length the Weissenberg number is defined as $Wi=\dot{\gamma}\tau_r$.

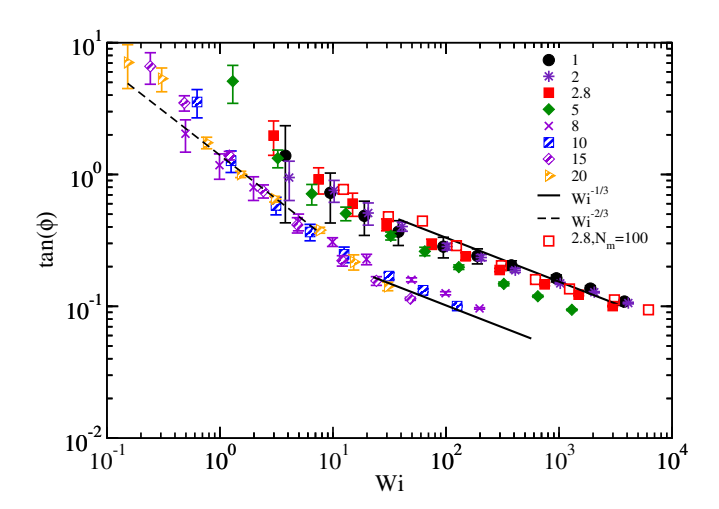


FIG. 8. Alignment of PEs with the shear flow as a function of the Weissenberg number for the various Bjerrum lengths (see legend). Dashed and solid lines indicate the power-law regimes $Wi^{-2/3}$ (Wi < 10) and $Wi^{-1/3}$ (Wi > 50), respectively. Open symbols (\square) correspond to results for the polymer length $N_m = 100$ at $l_B = 2.8$.

coiled states. Figure 9 displays snapshots of various conformations, which are numbered from 1 to 7. The conformations are distinguished by two parameters, the average fraction of overlapping monomers in *x*-direction, and their average distance, defined as

$$N_o = \sum_{i=1}^{N_m} \sum_{j=i+1}^{R_{ij}^x} N_{ij} \; ; \; R_{mm} = \frac{1}{N_o} \sum_{k=1}^{N_o} R_{ij}^x, \tag{10}$$

where R_{ij}^x is the distance between monomers along the x-direction, and will be non-zero only for $N_{ij} = 1$ if $|R_{ij}^x| \le \sigma/2$.

PLEASE CITE THIS ARTICLE AS DOI: 10.1122/8.0000085

No.	Range of n_a	Range of R _{mm}
1	$n_a < 0.1$	
2	$0.1 < n_a < 0.3$	
3	$0.3 < n_a < 0.7$	$R_{mm} < 2.2$
4	$0.3 < n_a < 0.7$	$R_{mm} > 2.2$
5	$0.7 < n_a < 0.1.5$	$R_{mm} < 2.2$
6	$0.7 < n_a < 0.1.5$	$R_{mm} > 2.2$
7	$1.5 < n_a$	

TABLE I. Definition of the various PE conformations: Extended states (1), semi-folded (2), closed (3) and open (4) U-shape conformations, closed (5) and open (6) S-shape or hair-pin conformations, and coil or collapsed globule conformations (7).

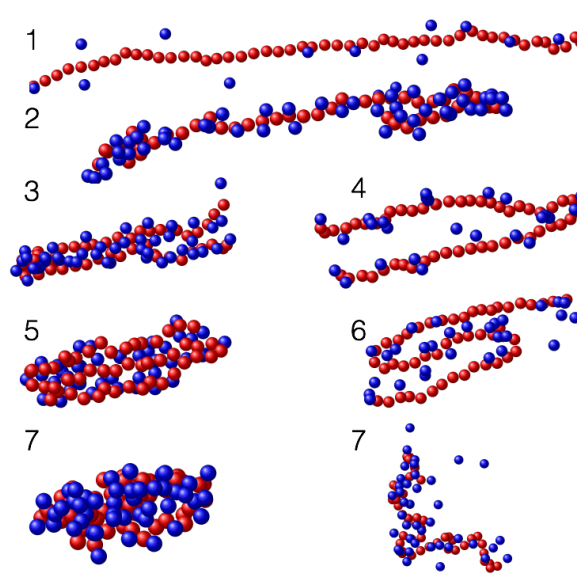


FIG. 9. Illustration of polyelectrolytes and their counterions for the extended state (1), semi-folded state (2), closed (3) and open (4) U-shape conformations, closed (5) and open (6) S-shape or hair-pin conformations, and coil and collapsed globule conformations (7). Movies illustrating the various confirmations are provided in the supplementary material for various l_B .

Importantly, summation over k in the second equation is only over those pairs with $R_{ij}^x < \sigma/2$. The classification proceeds then as follows (cf. Tab. I): If the fraction of overlapping monomer is $n_o = N_o/N_m < 0.1$, its an extended or stretched state, in the range $0.1 < n_o < 0.3$ the chain is in a partially folded state, for $0.3 < n_o < 0.7$ and $R_{mm} > 2.2$ in a U-shape conformation, and if $R_{mm} < 2.2$ in a collapsed conformation of U-type of overlapping PE parts. Similarly, for $0.7 < n_o < 1.5$ and $R_{mm} < 2.2$ the PE is of S-shape, and for $R_{mm} > 2.2$ the PE is in a hairpin open or closed state. Furthermore, coil or globule states strongly overlap in x-direction, which we identify in the range $n_o > 1.5$. In addition, we impose the condition that in the coil state $R_{cx} = \sum_{i,j=1}^{N_m} \langle (R_i - R_j)^2 \rangle$ is large, whereas it is small in the globular state, which we count in the same category (cf. Fig.11) Furthermore, the coil and globule state pertain large overlap values $n_0 > 1.5$; however, the two states

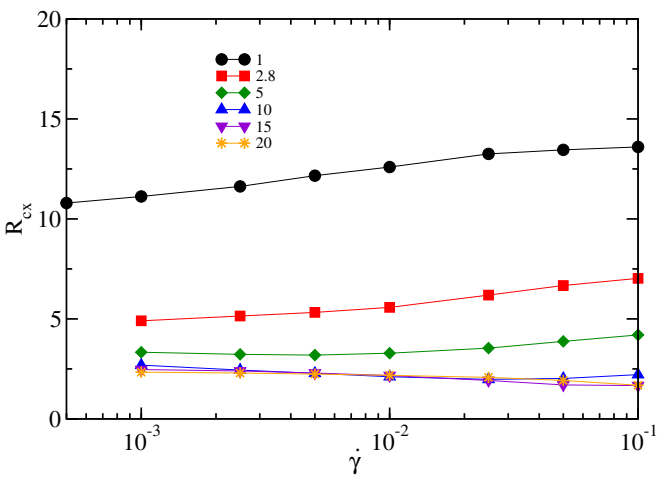


FIG. 10. Average distance of counterions from monomers as function of shear rate for various Bjerrum lengths, provided that their x-positions overlap is in the range $|R_{ij}| < \sigma/2$ with any monomer.

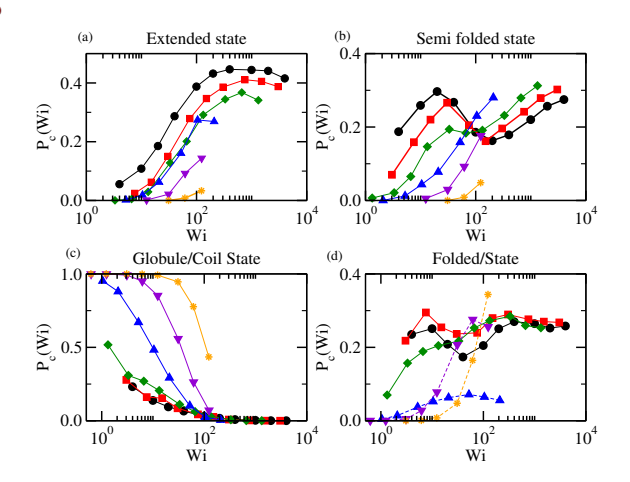


FIG. 11. Probability distribution function $P_c(Wi)$ of the various polymer states as a function of Wi for $l_B=1,\ 2.8,\ 5,\ 10,\ 15,\ and\ 20.$ The color code and symbols are the same as in Fig. 3. (d) Displays probability distributions functions of polyelectrolyte conformations in state 4 for $l_B=1,\ 2.8,\$ and 5, and state 5 for $l_B=10,\ 15,\$ and 20.

are mutually exclusive at a particular Bjerrum length, hence, we consider the latter sates as the same class. However, they can be distinguished by the average distance of counterions from the monomers when required. For clarification, these definitions are summarized in Tab. I. The average distance of the counterions from the monomers is nearly unperturbed by shear flow for $l_B \gtrsim 10$. This suggest that counterions are tightly bound to a PE even in strong flows, as in configurations 3, 5, and 7 in Fig. 9. The distance weakly increases with increasing shear rate for Bjerrum lengths $l_B < 10$. Figure 11 presents a more quantitative characterization, and indicates the higher probabilities of (c) globular and (d) folded states (state 5 for $l_B \gtrsim 10$ and state 4 for $l_B < 10$).

PLEASE CITE THIS ARTICLE AS DOI: 10.1122/8.0000085

πάντα

V. TUMBLING DYNAMICS

Polymers in shear flow exhibit an intriguing cyclic stretching and collapse dynamics denoted as tumbling, where the whole chain performs a rotational motion.^{2,16,18,36,62,63,77} In order to determine a characteristic tumbling time for PEs, their overall rotational motion is quantified with the help of the magnitude of the end-to-end vector, and the projection of the end-to-end vector onto the flow direction,

$$\cos \theta = \frac{\hat{x} \cdot R_e}{|R_e|},\tag{11}$$

where \hat{x} is the unit vector in the flow direction. Figure 12(a) provides an example for the time dependence of R_e and $\cos \theta$. Both quantities show a cyclic, but non-periodic motion. We define the tumbling time τ_t as average over many periods, where θ changes by 2π . The calculated tumbling times are displayed in Fig. 12(b) for various l_B . Evidently, coiled and globular PEs exhibit a distinctly different tumbling behavior. Universal behavior is obtained for $l_R < 3$, where τ_t decrease with increasing Weissenberg number according to the powerlaw $\tau_t \sim W i^{-\tilde{2}/3}$, consistent with the dependence of neutral polymers. 2,18,63 However, for $l_B \gtrsim 5$ a plateau-type regime appears for $l_B = 8$, 10, and 15 in the vicinity of $Wi = 10^2$. A plateau may also be present for $l_B = 20$ at higher Weissenberg numbers not considered in this study. The difference in the tumbling dynamics is related to the globular state of the PE. In the regime $Wi \lesssim 50$, the tumbling time is larger than the relaxation time τ_r ($\tau_t/\tau_r > 1$), i.e., the reorientation of a globule is slower than the relaxation of the end-to-end vector. This suggest that tumbling is not governed by the relaxation of the polymer, but rather by the rotation of the whole globule. In the plateau regime, $\tau_t/\tau_r \approx 1$, strong shear-induced conformational changes occur, which lead to large fluctuations of the magnitude of the end-to-end vector (cf. Fig. 4). Here, tumbling and end-to-end vector relaxation are strongly linked, and the relaxation of the end-to-end vector depends only weakly on shear. In the asymptotic limit of $Wi \gg 1$, even PEs at large l_B show conformations similar to those of neutral systems and their tumbling times become similar.

We like to stress that hydrodynamic interactions play a role in the tumbling motion of polyelectrolytes. Already free-draining polyelectrolytes exhibit deviations in the dependence of the tumbling time on the Weissenberg number from that of neutral polymers, however, the plateau for $l_B \approx 10$ is far less pronounced for free-draining polyelectrolytes.

VI. SUMMARY

In this article, we have presented results for the conformational and dynamical properties of polyelectrolytes in the presence of explicit counterions under shear flow using coarse-grained mesoscale hydrodynamics simulations. The conformations of charged polymers are strongly influenced by shear similar to those of neutral polymers. However, distinct differences emerge for strong Coulomb interactions, where counterions are condensed. In general, counterions display

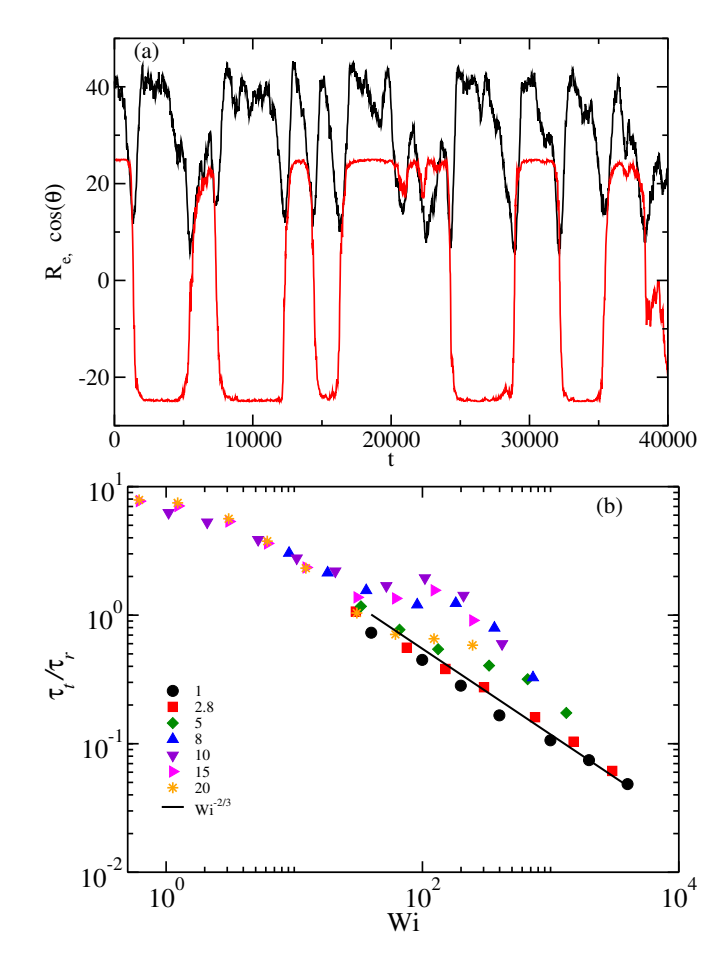


FIG. 12. (a) Magnitude of the end-to-end vector, R_e , (black) and the projection of R_e , $\cos\theta$, (red) onto the flow direction for $l_B=1$ and Wi=379. Note that $\cos\theta$ is multiplied by a factor of 25 for better visibility. (b) Normalized tumbling time τ_l as a function of the Weissenberg number for various Bjerrum lengths as indicated in the legend. The slope of the power-law line is -2/3. Note that the Weissenberg number is $Wi=\dot{\gamma}\tau_r$.

a similar dynamics as the PEs. However, there distribution is strongly influenced by shear flow in the limit of weak electrostatic attractions. In contrast, in the regime where they are condensed, $l_B\gg 1$, electrostatics dominates over forces exerted by flow, and the counterions closely follow the dynamics of the monomers, remaining always attached to a polymer. Shear-induced polymer alignment suggests two different power-law regimes, $\tan\phi\sim Wi^{-\beta}$, with the exponents $\beta=2/3$ in the weak flow regime and $\beta=1/3$ for strong flows, where the weak-flow exponent is different from that of neutral polymers.

We have identified seven distinct PE conformations under shear flow. Their respective probabilities suggest that globular chains ($l_B > 5$) are most often found in closed conformations of S-shape, U-shape, or in collapsed states. However, for coiled PEs extended states, and open S- and U-shape conformations are dominant.

Strongly charged PEs exhibit a distinct tumbling dynamics. For $l_B < 5$, tumbling is similar to neutral polymers, with tum-

PLEASE CITE THIS ARTICLE AS DOI: 10.1122/8.0000085

bling times decreasing with increasing Weissenberg number as $Wi^{-2/3}$. However, for $l_B > 5$, the globular chains exhibit a plateau-like regime for 50 < Wi < 500. This behavior is governed by an interplay of attractive interactions mediated by condensed counterions and external shear flow leading to extended polymer conformations. Here, the nonequilibrium polymer conformations are rather different from those of neutral polymers, as is illustrated by the various shapes presented in Fig. 9.

Our simulation studies reveal a markedly different shear response of PEs in the presence of counterions compared to neutral polymers, ^{36,47,63,67} specifically for stronger Coulombinteractions, where globular conformations are assumed. Typically, the Bjerrum lengths of strongly charged synthetic and biological polymers are in the range $l_B = 2 - 4$ under physiological conditions for monovalent counterions⁴. For example, the Bjerrum length of DNA is $l_B \approx 0.7nm$ in water and the bond length is 0.34nm, which yields a scaled Bjerrum length of $l_B/l_0 = 2$. Hence, such PEs exhibit features similar to neutral polymers under shear. Larger Bjerrum lengths are hardly feasible in experiments on DNA or Polystyrene sulfonate (PSS). It can be varied approximately two fold via changing the dielectric constant by addition of alcohol, acetone, or ethylene glycol in aqueous solution⁷⁸. However, stronger electrostatic interactions, with scaled Bjerrum length approx. 10 to study particular effects of coil-unfolding under shear, can be achieved by multivalent monomers and/or counterions. Such kinds of systems have hardly been analyzed so for, specifically under shear flow. It is important to note that although the bulk dielectric constant of the fluid is large, it can be as low as $\varepsilon_r \approx 3 - 10$ in the vicinity of a bond^{4,79}.

The dielectric permittivity near a macromolecule is much lower than the bulk value. A careful analysis, assuming local variation of permittivity, reveals significant qualitative change in the dynamics of polyelectrolytes⁸⁰. With such variations, coarse-grained simulations are even able to quantitatively reproduce results of explicit-solvent atomistic simulation results. Further studies are required to resolve effects of local variations in the dielectric constant and the intricate interplay of polymer structures and explicit counterions^{80,81}, specifically in the globular limit, where ion-ion correlations are dominant.

ACKNOWLEDGMENT

SPS acknowledges DST SERB New Delhi, Grant No. YSS/2015/000230 for the financial support, and computational time by HPC facility at IISER Bhopal.

VII. SUPPLEMENTARY MATERIAL

SI-Movie-1: A movie displaying dynamics of a polyelectrolyte's conformations under shear for $l_B = 2.8$ at Weissenberg number Wi = 3. SI-Movie-2: A movie displaying dynamics of a polyelectrolyte's conformations under shear for $l_B = 2.8$ at Weissenberg number Wi = 1470. SI-Movie-3:

A movie displaying dynamics of a globular polyelectrolyte's conformations under shear for $l_B=10$ at Weissenberg number Wi=0.2. SI-Movie-4: A movie displaying dynamics of a globular polyelectrolyte's conformations under shear for $l_B=10$ at Weissenberg number Wi=104.

- ¹J. Hur, E. S. G. Shaqfeh, H. P. Babcock, D. E. Smith, and S. Chu, "Dynamics of dilute and semidilute dna solutions in the start-up of shear flow," J. Rheol. **45**, 421 (2001).
- ²C. M. Schroeder, R. E. Teixeira, E. S. G. Shaqfeh, and S. Chu, "Characteristic periodic motion of polymers in shear flow," Phys. Rev. Lett. 95, 018301 (2005).
- ³M. Doi and S. F. Edwards, *The Theory of Polymer Dynamics* (Oxford University press, New York, 1986).
- ⁴M. Muthukumar, *Polymer translocation* (Taylor & Francis US, 2011).
- ⁵I. Rubenstein and S. B. Leighton, "The influence of rotor speed on the sedimentation behavior in sucrose gradients of high molecular weight dna's," Biophysical chemistry 1, 292–299 (1974).
- ⁶R. W. Clark and C. S. Lange, "A quantitative test of zimm's model for the rotor-speed-department sedimentation of linear dna molecules," Biopolymers: Original Research on Biomolecules 19, 945–964 (1980).
- ⁷X. Schlagberger and R. R. Netz, "Anomalous polymer sedimentation far from equilibrium," Physical review letters 98, 128301 (2007).
- ⁸X. Schlagberger and R. R. Netz, "Anomalous sedimentation of self-avoiding flexible polymers," Macromolecules 41, 1861–1871 (2008).
- ⁹S. P. Singh, G. Gompper, and R. G. Winkler, "Steady state sedimentation of ultrasoft colloids," The Journal of chemical physics **148**, 084901 (2018).
- ¹⁰D. Hoagland, E. Arvanitidou, and C. Welch, "Capillary electrophoresis measurements of the free solution mobility for several model polyelectrolyte systems," Macromolecules 32, 6180–6190 (1999).
- ¹¹K. Grass, U. Böhme, U. Scheler, H. Cottet, and C. Holm, "Importance of hydrodynamic shielding for the dynamic behavior of short polyelectrolyte chains," Phys. Rev. Lett. **100**, 096104 (2008).
- ¹²K. Grass and C. Holm, "Importance of hydrodynamic shielding for the dynamic behavior of short polyelectrolyte chains," Soft Matter 5, 2079 (2009).
- ¹³S. Frank and R. Winkler, "Polyelectrolyte electrophoresis: Field effects and hydrodynamic interactions," EPL (Europhysics Letters) 83, 38004 (2008).
- ¹⁴S. Frank and R. G. Winkler, "Mesoscale hydrodynamic simulation of short polyelectrolytes in electric fields," The Journal of chemical physics 131, 234905 (2009).
- ¹⁵C. Aust, M. Kröger, and S. Hess, "Structure and dynamics of dilute polymer solutions under shear flow via nonequilibrium molecular dynamics," Macromolecules 32, 5660 (1999).
- ¹⁶S. Gerashchenko and V. Steinberg, "Statistics of tumbling of a single polymer molecule in shear flow," Physical review letters 96, 038304 (2006).
- ¹⁷A. Balducci, C.-C. Hsieh, and P. Doyle, "Relaxation of stretched dna in slitlike confinement," Physical review letters 99, 238102 (2007).
- ¹⁸R. G. Winkler, "Semiflexible polymers in shear flow," Phys. Rev. Lett. 97, 128301 (2006)
- ¹⁹S. P. Singh, A. Chatterji, G. Gompper, and R. G. Winkler, "Dynamical and rheological properties of ultrasoft colloids under shear flow," Macromolecules 46, 8026–8036 (2013).
- ²⁰S. P. Singh, A. Chatterji, R. G. Winkler, and G. Gompper, "Conformational and dynamical properties of ultra-soft colloids in semi-dilute solutions under shear flow," J. Phys.: Condens. Matter 24, 464103 (2012).
- ²¹A. Alexander-Katz, M. F. Schneider, S. W. Schneider, A. Wixforth, and R. R. Netz, "Shear-Flow-Induced Unfolding of Polymeric Globules," (2006), 10.1103/PhysRevLett.97.138101.
- ²²W. Factor and Z. M. Ruggeri, "Perspectives Series: Cell Adhesion in Vascular Biology von Willebrand Factor," J. Clin. Invest 99, 559–564 (1997).
- ²³ K. Radhakrishnan and S. P. Singh, "Force driven transition of a globular polyelectrolyte," The Journal of chemical physics 151, 174902 (2019).
- ²⁴R. Chelakkot, R. G. Winkler, and G. Gompper, "Migration of semiflexible polymers in microcapillary flow," EPL (Europhysics Letters) **91**, 14001 (2010)
- ²⁵D. Steinhauser, S. Köster, and T. Pfohl, "Mobility gradient induces cross-streamline migration of semiflexible polymers," ACS Macro Letters 1, 541–545 (2012).
- ²⁶R. G. Larson, The structure and rheology of complex fluids (Oxford University Press, Oxford, NY, 1999).

the online version of record will be different from this version once it has been copyedited and typeset

PLEASE CITE THIS ARTICLE AS DOI: 10.1122/8.0000085

accepted manuscript. However,

This is the author's peer reviewed,

- ²⁷R. B. Bird, C. F. Curtiss, R. C. Armstrong, and O. Hassager, *Dynamics of polymeric liquids: Kinetic theory* (Wiley, New York, 1987).
- ²⁸S. Kesselheim, W. Müller, and C. Holm, "Origin of current blockades in nanopore translocation experiments," Phys. Rev. Lett. **112**, 018101 (2014).
- ²⁹M. S. Kamal, A. S. Sultan, U. A. Al-Mubaiyedh, and I. A. Hussein, "Review on polymer flooding: Rheology, adsorption, stability, and field applications of various polymer systems," Polymer Reviews 55, 491–530 (2015).
- ³⁰N. A. Peppas, K. B. Keys, M. Torres-Lugo, and A. M. Lowman, "Poly(ethylene glycol)-containing hydrogels in drug delivery," J. Contr. Release 62, 81–87 (1999).
- ³¹L. Y. Qiu and Y. H. Bae, "Polymer architecture and drug delivery," Pharmaceutical Res. 23, 1–30 (2006).
- ³²J. T. Wiltshire and G. G. Qiao, "Recent advances in star polymer design: Degradability and the potential for drug delivery," Austral. J. Chem. 60, 699–705 (2007).
- ³³S. W. Schneider, S. Nuschele, A. Wixforth, C. Gorzelanny, A. Alexander-Katz, R. R. Netz, and M. F. Schneider, "Shear-induced unfolding triggers adhesion of von Willebrand factor fibers," Tech. Rep. (2007).
- ³⁴C.-C. Huang, R. G. Winkler, G. Sutmann, and G. Gompper, "Semidilute polymer solutions at equilibrium and under shear flow," Macromolecules 43, 10107–10116 (2010).
- ³⁵C.-C. Huang, G. Gompper, and R. G. Winkler, "Non-equilibrium relaxation and tumbling times of polymers in semidilute solution," J. Phys.: Condens. Matter 24, 284131 (2012).
- ³⁶S. Singh, R. K. Singh, D. Das, and S. Kumar, "Kinetics of polymer tumbling in shear flow: A coarse-grained description," Phys. Rev. E 99, 030501 (2019).
- ³⁷L. B. Weiss, C. N. Likos, and A. Nikoubashman, "Spatial demixing of ring and chain polymers in pressure-driven flow," Macromolecules **52**, 7858– 7869 (2019).
- ³⁸R. Kekre, J. E. Butler, and A. J. Ladd, "Role of hydrodynamic interactions in the migration of polyelectrolytes driven by a pressure gradient and an electric field," Physical Review E 82, 050803 (2010).
- ³⁹N. Hoda and S. Kumar, "Brownian dynamics simulations of polyelectrolyte adsorption in shear flow with hydrodynamic interaction," The Journal of chemical physics **127**, 234902 (2007).
- ⁴⁰N. Hoda and S. Kumar, "Kinetic theory of polyelectrolyte adsorption in shear flow," Journal of Rheology **51**, 799–820 (2007).
- ⁴¹N. Hoda and S. Kumar, "Brownian dynamics simulations of polyelectrolyte adsorption in shear flow: effects of solvent quality and charge patterning," The Journal of chemical physics 128, 164907 (2008).
- ⁴²P. G. de Gennes, Scaling concepts in polymer physics (Cornell University Press, Ithaca, 1979).
- ⁴³R. G. Winkler, M. Gold, and P. Reineker, "Collapse of polyelectrolyte macromolecules by counterion condensation and ion pair formation: a molecular dynamics simulation study," Physical review letters 80, 3731 (1998).
- ⁴⁴M. Muthukumar and C. Kong, "Simulation of polymer translocation through protein channels," Proceedings of the National Academy of Sciences 103, 5273–5278 (2006).
- ⁴⁵A. M. Tom, S. Vemparala, R. Rajesh, and N. V. Brilliantov, "Mechanism of chain collapse of strongly charged polyelectrolytes," Phys. Rev. Lett. 117, 147801 (2016).
- ⁴⁶S. Liu and M. Muthukumar, "Langevin dynamics simulation of counterion distribution around isolated flexible polyelectrolyte chains," The Journal of chemical physics 116, 9975–9982 (2002).
- ⁴⁷S. P. Singh and M. Muthukumar, "Electrophoretic mobilities of counterions and a polymer in cylindrical pores," The Journal of chemical physics **141**, 09B610_1 (2014).
- ⁴⁸J. Tang, N. Du, and P. S. Doyle, "Compression and self-entanglement of single dna molecules under uniform electric field," Proceedings of the National Academy of Sciences (2011).
- ⁴⁹C. Zhou, W. W. Reisner, R. J. Staunton, A. Ashan, R. H. Austin, and R. Riehn, "Collapse of dna in ac electric fields," Physical review letters
- ⁵⁰S. Nedelcu and J.-U. Sommer, "Simulations of polyelectrolyte dynamics in an externally applied electric field in confined geometry," The Journal of chemical physics 133, 244902 (2010).
- 51 M. Arca, J. E. Butler, and A. J. Ladd, "Transverse migration of polyelectrolytes in microfluidic channels induced by combined shear and electric

- fields," Soft Matter 11, 4375-4382 (2015).
- ⁵²A. J. Ladd, "Electrophoresis of sheared polyelectrolytes," Molecular Physics 116, 3121–3133 (2018).
- ⁵³S. J. Park, A. Shakya, and J. T. King, "Depletion layer dynamics of polyelectrolyte solutions under poiseuille flow," Proceedings of the National Academy of Sciences 116, 16256–16261 (2019).
- ⁵⁴S. Dutta, K. D. Dorfman, and S. Kumar, "Shear-induced desorption of isolated polymer molecules from a planar wall," ACS Macro Letters 4, 271– 274 (2015).
- ⁵⁵G.-L. He, R. Messina, H. Löwen, A. Kiriy, V. Bocharova, and M. Stamm, "Shear-induced stretching of adsorbed polymer chains," Soft Matter 5, 3014–3017 (2009).
- ⁵⁶Y. Li, K.-W. Hsiao, C. A. Brockman, D. Y. Yates, R. M. Robertson-Anderson, J. A. Kornfield, M. J. San Francisco, C. M. Schroeder, and G. B. McKenna, "When ends meet: Circular dna stretches differently in elongational flows," Macromolecules 48, 5997–6001 (2015).
- ⁵⁷L. Liu, J. Chen, and L. An, "Individual circular polyelectrolytes under shear flow," The Journal of chemical physics 149, 163316 (2018).
- ⁵⁸ K. Jayasree, R. Kumar Manna, D. Banerjee, and P. S. Kumar, "Dynamics of a polyelectrolyte in simple shear flow," The Journal of chemical physics 139, 224902 (2013).
- ⁵⁹R. Kapral, "Multiparticle collision dynamics: Simulation of complex systems on mesoscales," Adv. Chem. Phys. **140**, 89 (2008).
- ⁶⁰G. Gompper, T. Ihle, D. M. Kroll, and R. G. Winkler, "Multi-particle collision dynamics: a particle-based mesoscale simulation approach to the hydrodynamics of complex fluids," Adv. Polym. Sci. 221, 1–87 (2009).
- ⁶¹A. Alexander-Katz and R. Netz, "Dynamics and instabilities of collapsed polymers in shear flow," Macromolecules 41, 3363–3374 (2008).
- ⁶²R. Delgado-Buscalioni, "Cyclic motion of a grafted polymer under shear flow," Phys. Rev. Lett. **96**, 088303 (2006).
- ⁶³C.-C. Huang, G. Sutmann, G. Gompper, and R. G. Winkler, "Tumbling of polymers in semidilute solution under shear flow," EPL 93, 54004 (2011).
- ⁶⁴N. Hoda and R. G. Larson, "Brownian dynamics simulations of single polymer chains with and without self-entanglements in theta and good solvents under imposed flow fields," Journal of Rheology 54, 1061–1081 (2010).
- ⁶⁵ M. P. Allen and D. J. Tildesley, *Computer Simulation of Liquids* (Clarendon Press, Oxford, 1987).
- ⁶⁶D. R. Wheeler, N. G. F. Fuller, and R. L. Rowley, "Non-equilibrium molecular dynamics simulation of the shear viscosity of liquid methanol: adaptation of the ewald sum to lees-edwards boundary conditions," Molecular Physics 92, 55–62 (1997).
- ⁶⁷C.-C. Huang, A. Chatterji, G. Sutmann, G. Gompper, and R. G. Winkler, "Cell-level canonical sampling by velocity scaling for multiparticle collision dynamics simulations," J. Comp. Phys. 229, 168 (2010).
- ⁶⁸E. Allahyarov and G. Gompper, "Mesoscopic solvent simulations: Multiparticle-collision dynamics of three-dimensional flows," Phys. Rev. E 66, 036702 (2002).
- ⁶⁹T. Ihle and D. M. Kroll, "Stochastic rotation dynamics: A Galilean-invariant mesoscopic model for fluid flow," Phys. Rev. E 63, 020201(R) (2001).
- ⁷⁰A. W. Lees and S. F. Edwards, "The computer study of transport processes under extreme conditions," J. Phys. C 5, 1921–1928 (1972).
- ⁷¹E. Tüzel, M. Strauss, T. Ihle, and D. M. Kroll, "Transport coefficients for stochastic rotation dynamics in three dimensions," Physical Review E 68, 036701 (2003).
- ⁷²N. Kikuchi, C. Pooley, J. Ryder, and J. Yeomans, "Transport coefficients of a mesoscopic fluid dynamics model," The Journal of chemical physics 119, 6388–6395 (2003).
- ⁷³S.-Q. Wang, "Shear induced deformation of polymers: Calculation of radii of gyration," J. Chem. Phys. **92**, 7618 (1990).
- ⁷⁴C. Pierleoni and J.-P. Ryckaert, "Deformation and orientation of flexible polymers in solution under shear flow: A new picture of intermediate reduced shear rates," Macromolecules 28, 5097 (1995).
- ⁷⁵R. G. Winkler, "Conformational and rheological properties of semiflexible polymers in shear flow," J. Chem. Phys. **133**, 164905 (2010).
- ⁷⁶A. Alexander-Katz, H. Wada, and R. R. Netz, "Internal friction and nonequilibrium unfolding of polymeric globules," Physical review letters 103, 028102 (2009).
- ⁷⁷H. Kobayashi and R. Yamamoto, "Tumbling motion of a single chain in shear flow: A crossover from Brownian to non-Brownian behavior," Phys.

PLEASE CITE THIS ARTICLE AS DOI: 10.1122/8.0000085

Rev. E 81, 041807 (2010).

⁷⁸S. M. Mel'nikov, M. O. Khan, B. Lindman, and B. Jönsson, "Phase behavior of single dna in mixed solvents," Journal of the American Chemical Society **121**, 1130–1136 (1999).

⁷⁹Z. Li, R. Kumarasinghe, M. M. Collinson, and D. A. Higgins, "Probing the local dielectric constant of plasmid dna in solution and adsorbed on chemically graded aminosilane surfaces," The Journal of Physical Chemistry B

122, 2307–2313 (2018).

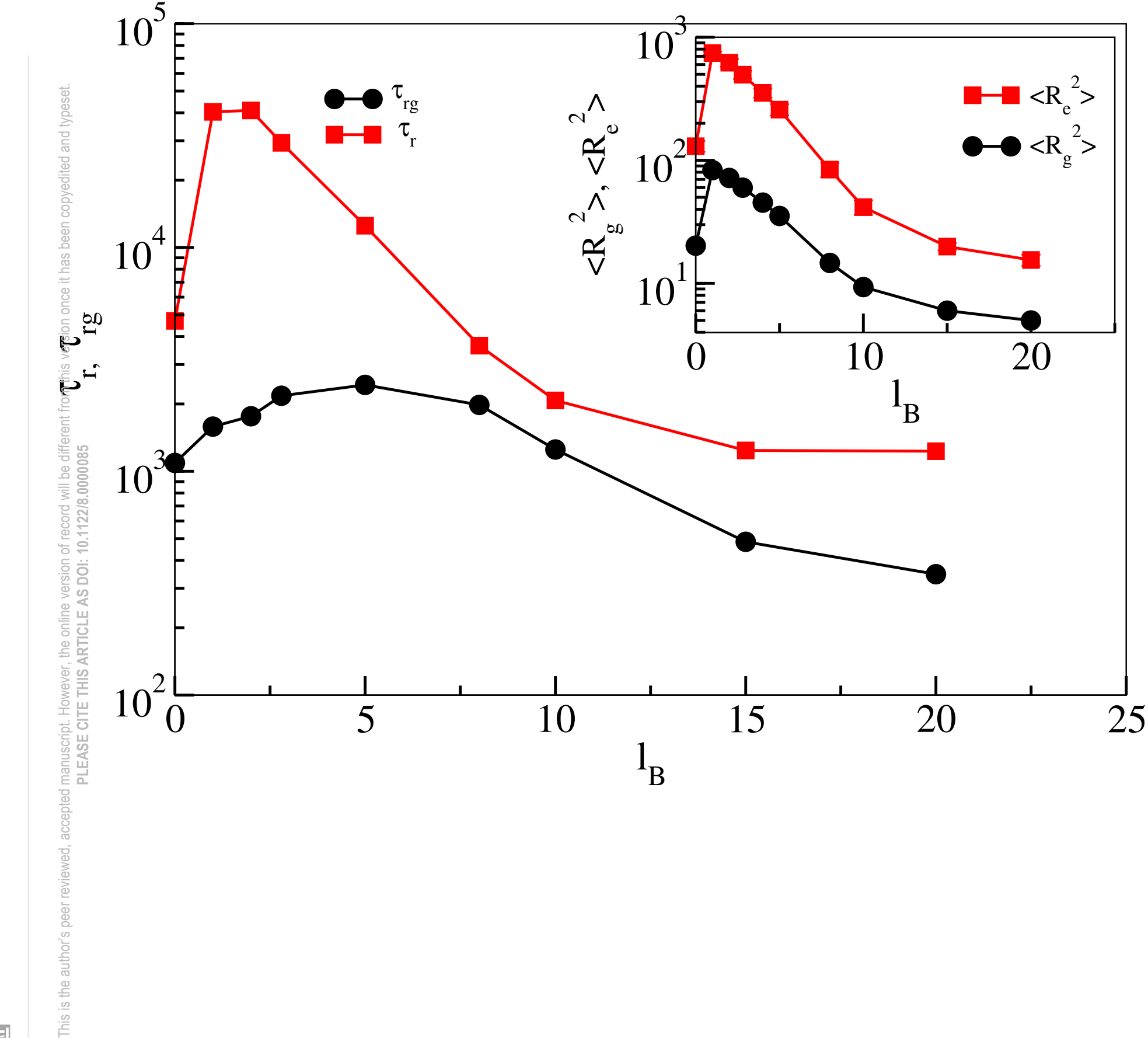
⁸⁰F. Fahrenberger, O. A. Hickey, J. Smiatek, and C. Holm, "The influence of charged-induced variations in the local permittivity on the static and dynamic properties of polyelectrolyte solutions," The Journal of chemical physics 143, 243140 (2015).

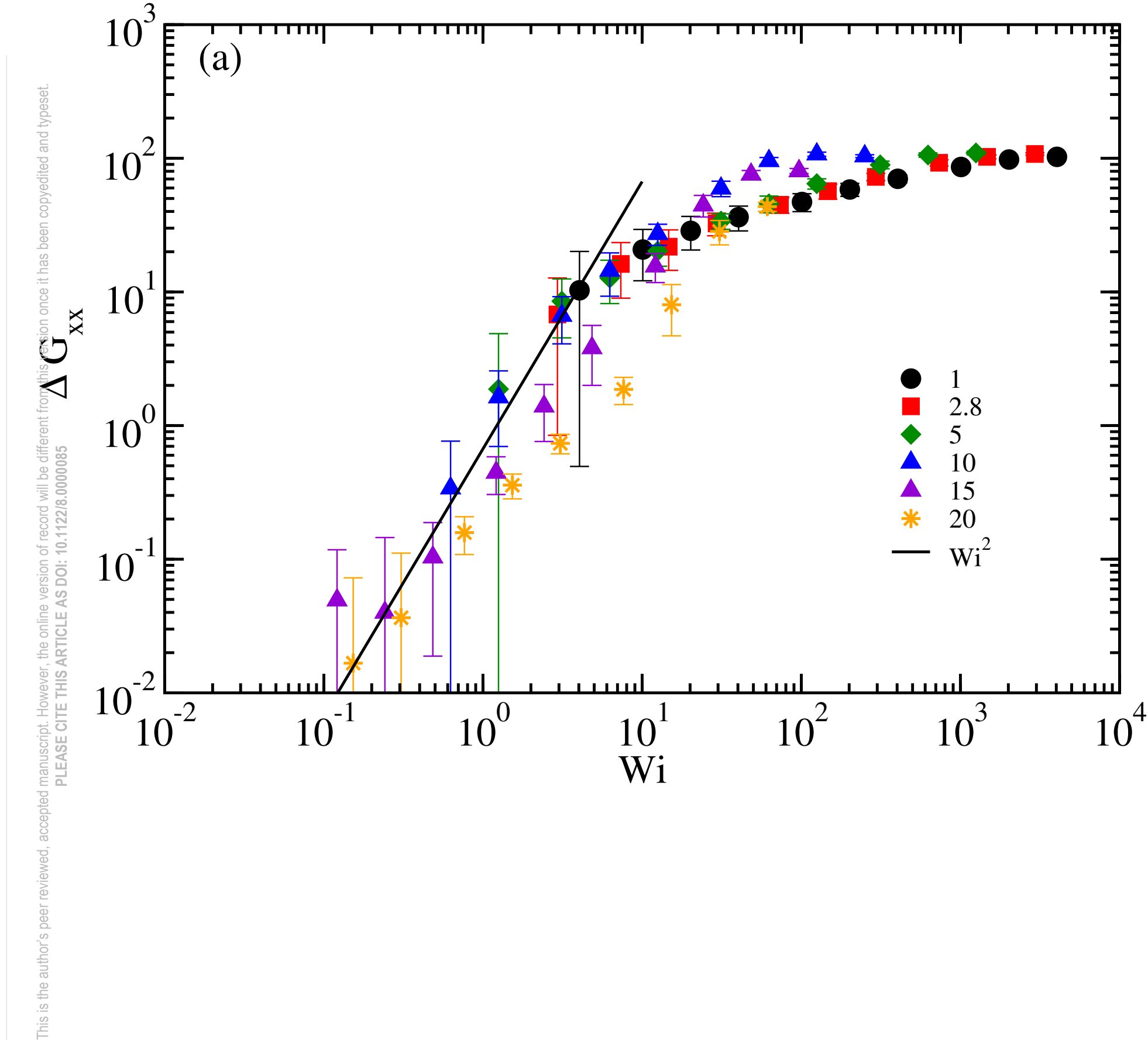
⁸¹N. Hoda and R. G. Larson, "Explicit-and implicit-solvent molecular dynamics simulations of complex formation between polycations and polyanions," Macromolecules 42, 8851–8863 (2009).



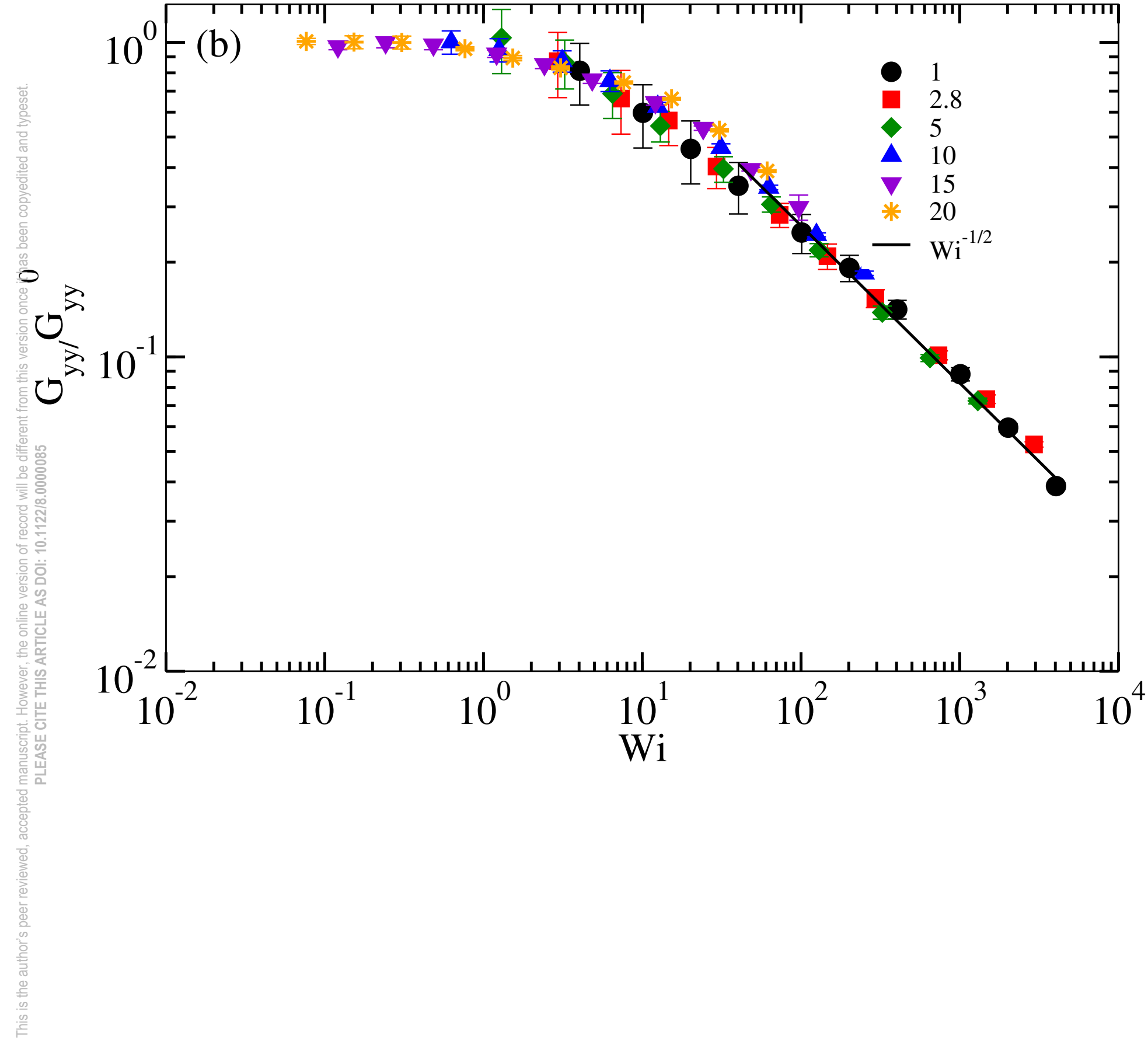
uscript. However, the online version of record will be different from this version once it has been copyedited and typeset.

ASE CITE THIS ARTICLE AS DOI: 10.1122/8.0000085 This is the author's peer reviev

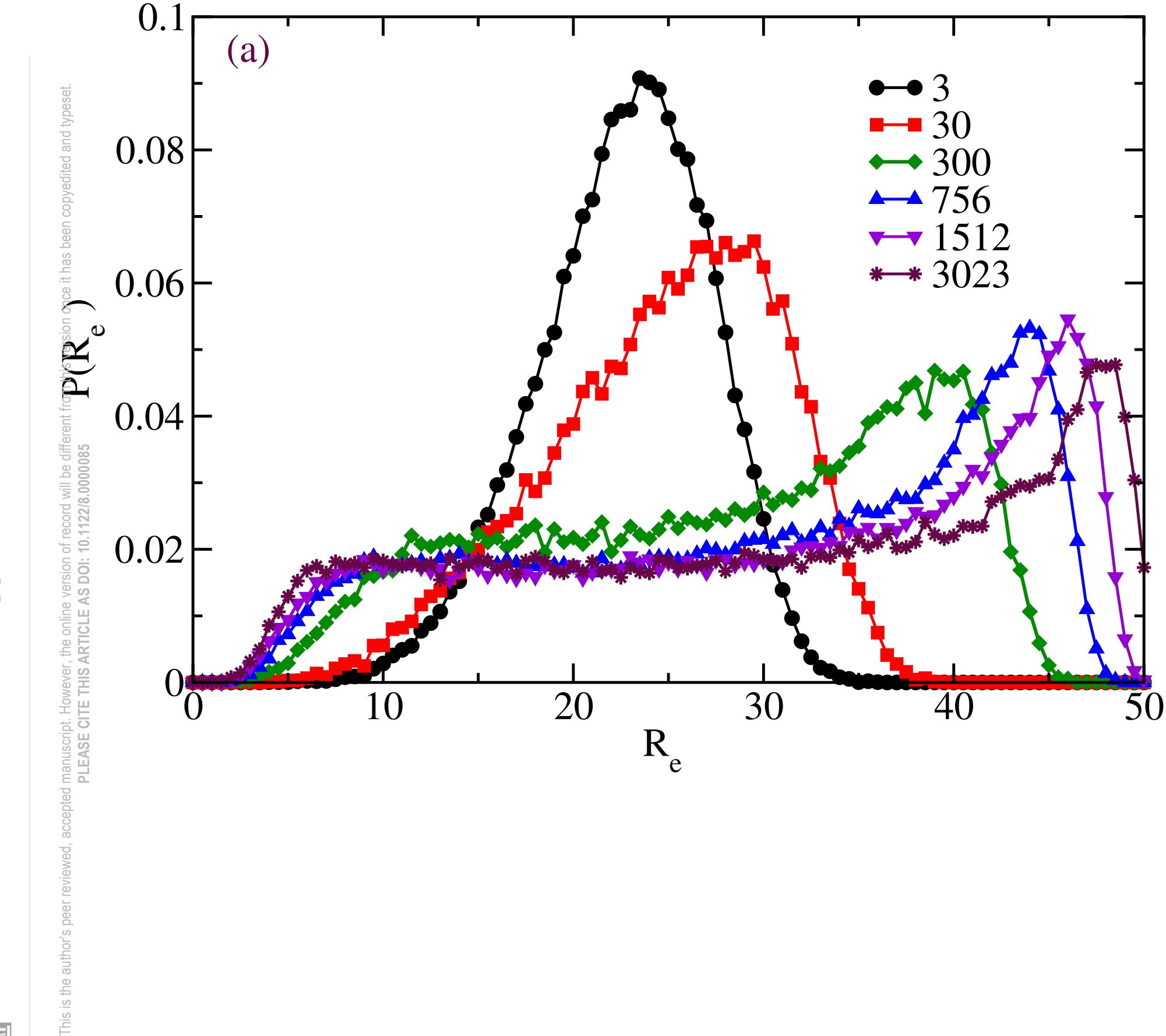


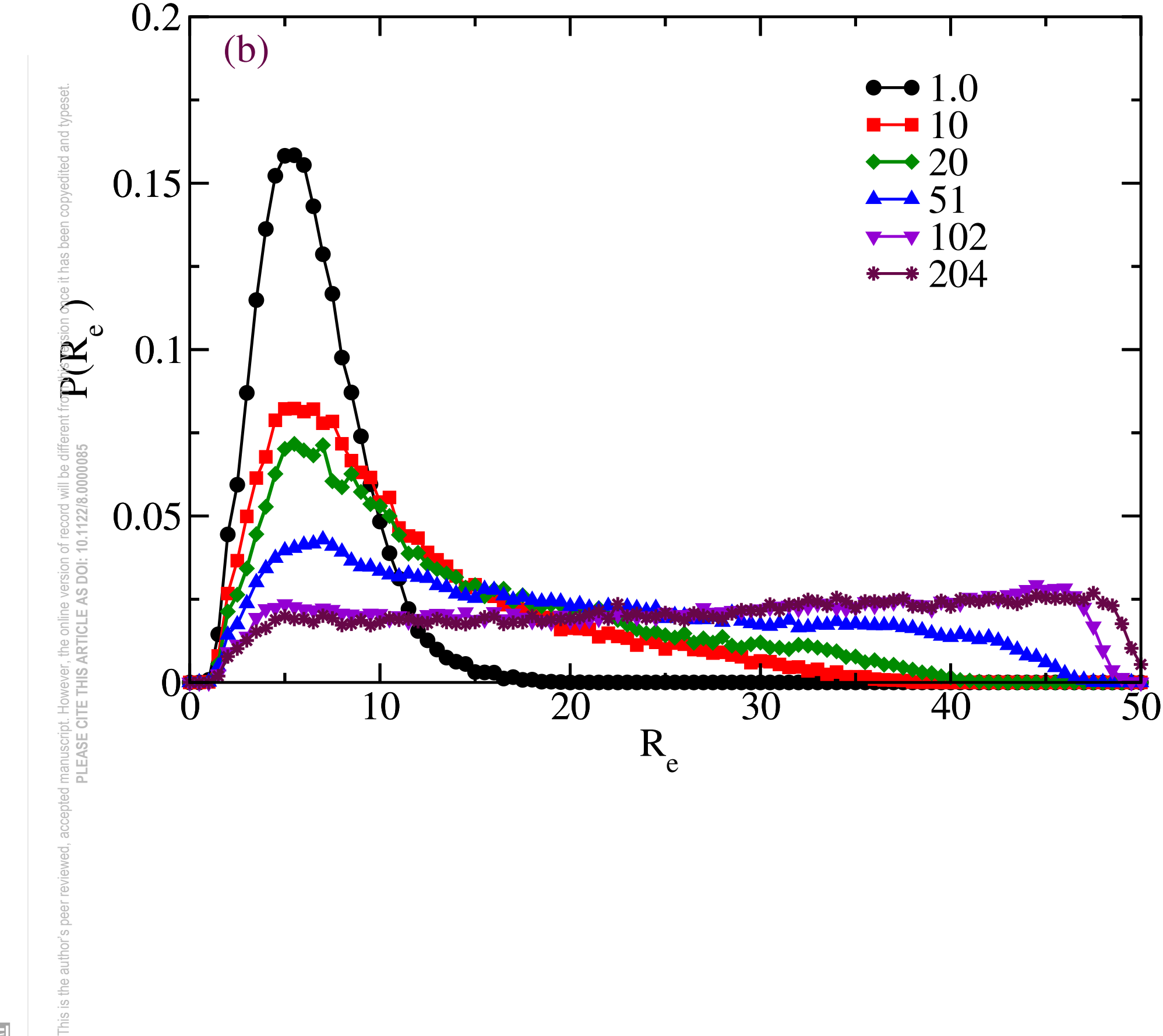








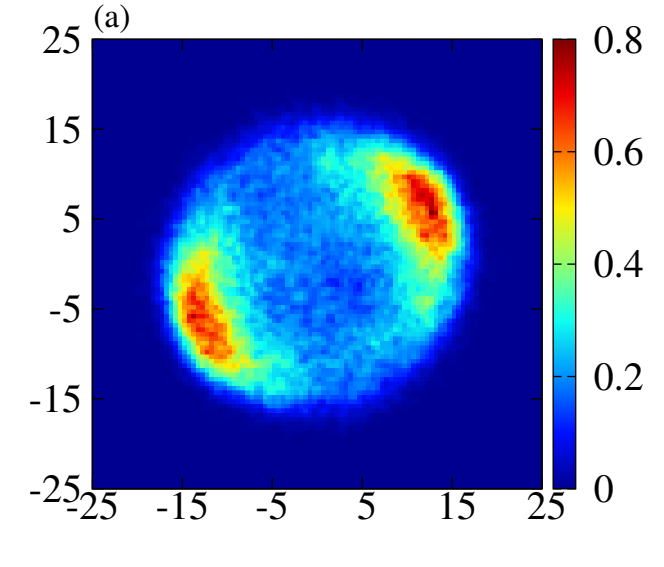




Journal of Rheology

This is the author's peer reviewed, accepted manuscript. However, the online version of record will be different from this version once it has been copyedited and typeset.

PLEASE CITE THIS ARTICLE AS DOI: 10.1122/8.0000085





Journal of Rheology

This is the author's peer reviewed, accepted manuscript. However, the online version of record will be different from this version once it has been copyedited and typeset.

PLEASE CITE THIS ARTICLE AS DOI: 10.1122/8.0000085

25 (b) 15 5 -5 -15 -25₂₅ -15 15 -5 5

1.0

0.5

0

25



Journal of Rheology

This is the author's peer reviewed, accepted manuscript. However, the online version of record will be different from this version once it has been copyedited and typeset.

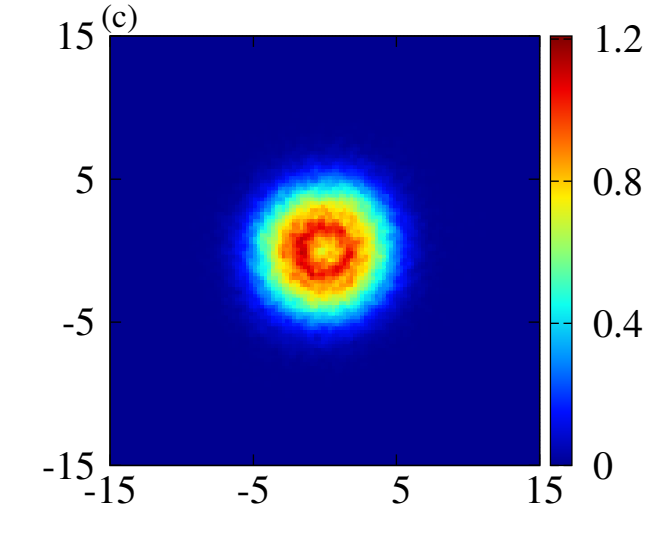
PLEASE CITE THIS ARTICLE AS DOI: 10.1122/8.0000085

15 (d) 5 0.4 0.3 0.2 0.1 0.1

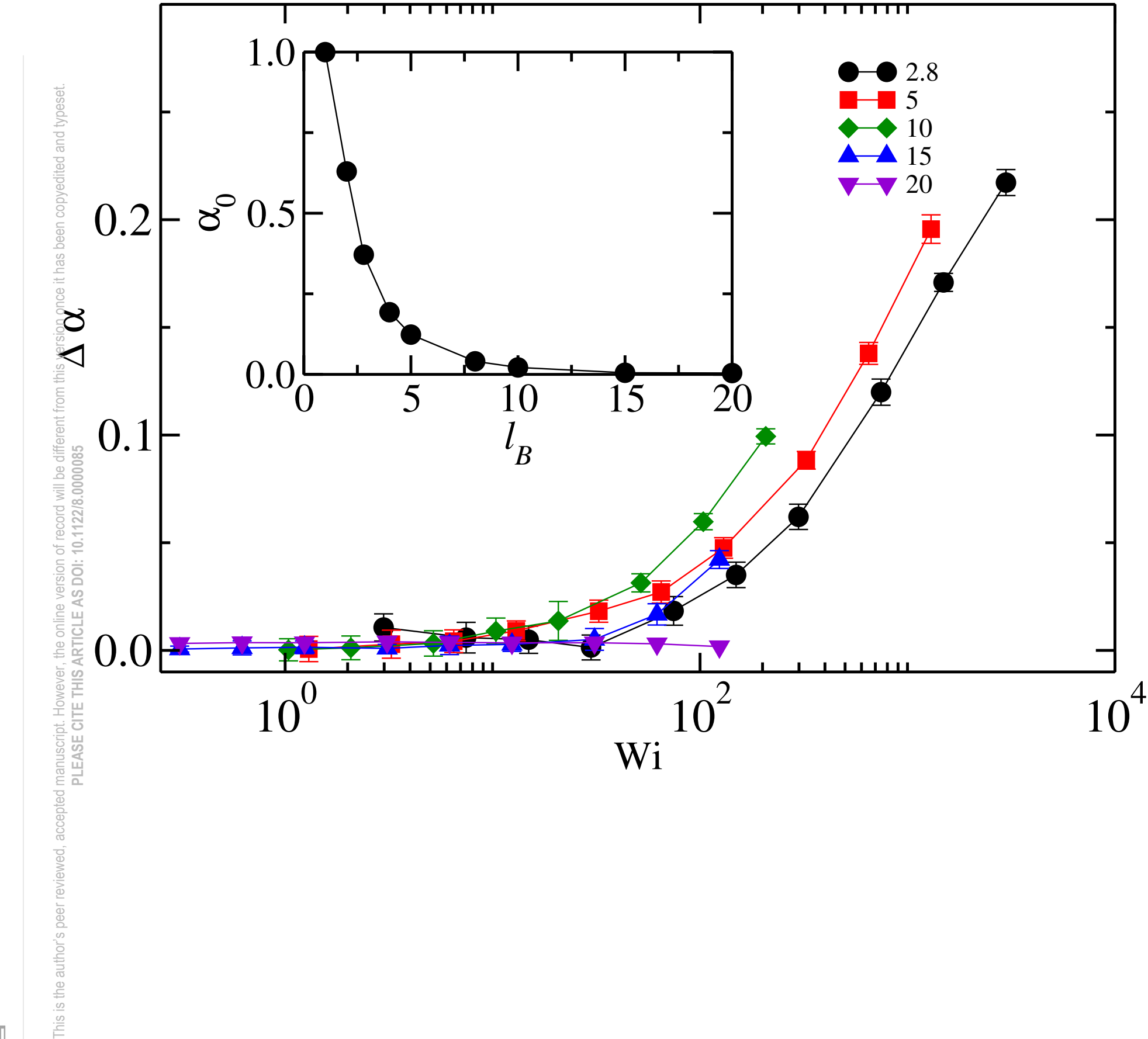


Journal of Rheology

This is the author's peer reviewed, accepted manuscript. However, the online version of record will be different from this version once it has been copyedited and typeset. PLEASE CITE THIS ARTICLE AS DOI: 10.1122/8.0000085









Journal of Rheology

15^(a)
5
-5
-15
-15
-5
5
1.5

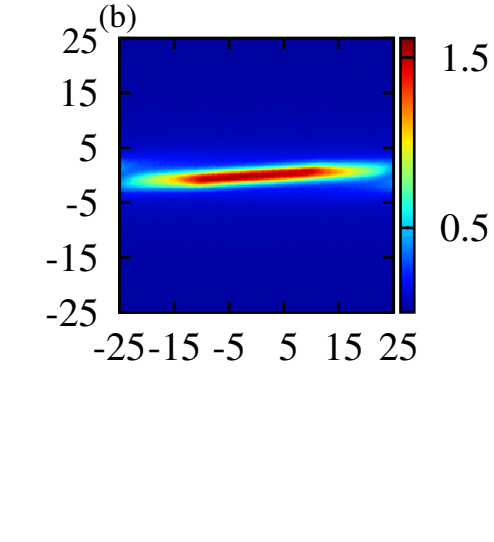
This is the author's peer reviewed, accepted manuscript. However, the online version of record will be different from this version once it has been copyedited and typeset.

PLEASE CITE THIS ARTICLE AS DOI: 10.1122/8.0000085



Journal of Rheology

This is the author's peer reviewed, accepted manuscript. However, the online version of record will be different from this version once it has been copyedited and typeset. PLEASE CITE THIS ARTICLE AS DOI: 10.1122/8.0000085

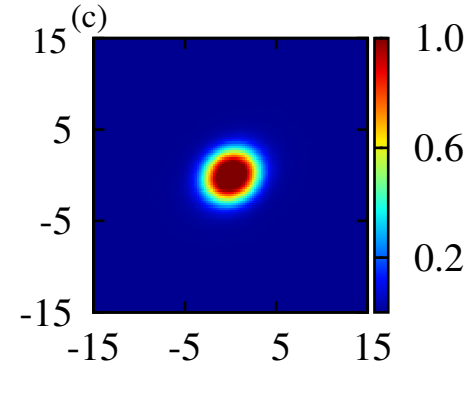




Journal of Rheology

This is the author's peer reviewed, accepted manuscript. However, the online version of record will be different from this version once it has been copyedited and typeset.

PLEASE CITE THIS ARTICLE AS DOI: 10.1122/8.0000085





Journal of Rheology

This is the author's peer reviewed, accepted manuscript. However, the online version of record will be different from this version once it has been copyedited and typeset.

PLEASE CITE THIS ARTICLE AS DOI: 10.1122/8.0000085

